EURASIAN PHYSICAL TECHNICAL JOURNAL

2025, Volume 22, No.2 (52)

https://doi.org/10.31489/2025N2/25-32

Received: 30/11/2024 Revised: 27/03/2025 Accepted: 12/05/2025 Published online: 30/06/2025

Research Article

UDC 535.37

PROPERTIES OF Ag/TiO_2 AND Ag/SiO_2 NANOPARTICLES AND THEIR EFFECT ON THE PHOTOCATALYTIC PROPERTIES OF A SEMICONDUCTOR NANOCOMPOSITE

Sharapov I., Omarova G., Sadykova A., Seliverstova E.*

Institute of Molecular Nanophotonics, Karaganda Buketov University, Karaganda, Kazakhstan

*Corresponding author: genia_sv@mail.ru

Abstract. *The optical properties and the electric field distribution around silver nanoparticles coated with TiO_2 or SiO_2 shell have been studied. It is demonstrated that the presence of a shell around a plasmonic nanoparticle leads to a bathochromic shift in the maximum of its absorption band. The maximum electric field intensity around metal nanoparticles is radially concentrated, predominantly near the surface of the nanoparticles. The quantum efficiency, representing the ratio of emitted photons to absorbed photons, is nearly 50% higher for Ag/TiO_2 nanoparticles compared to Ag/SiO_2. In the presence of Ag/TiO_2 and Ag/SiO_2 core/shell nanoparticles the photocatalytic activity of the TiO_2/rGO nanocomposite increases by 2.7 and 1.7 times, respectively. These changes are associated with improved charge transport properties of TiO_2/rGO and possible hot electron injection from the nanoparticles into the semiconductor.*

Keywords: plasmon, nanoparticles, optical properties, photocatalysis, nanocomposite.

1. Introduction

Localized surface plasmon resonance (LSPR) refers to the collective oscillation of conduction electrons in metallic nanoparticles (NPs) under the influence of external electromagnetic excitation [1]. This phenomenon has attracted significant attention from researchers due to its unique properties. For instance, the capability of plasmon NPs to efficiently absorb and scatter light in a various spectral ranges makes them highly promising for a wide variety of applications, including photocatalysis [2], optical devices [3], and solar energy [4]. Of particular interest for practical applications are core/shell nanostructures, where a metallic core, such as Ag or Au NPs, is surrounded by a dielectric or semiconductor shell. These structures exhibit several advantages over the monocomponent NPs. Specifically, the shell provides stability of the metallic core against external influences, enables control over local electromagnetic fields near the NPs, and modifies its interaction with incident radiation. Additionally, the shell can create conditions for efficient electron transfer [5] that is essential for photovoltaic processes, and optimize the spatial configuration between plasmon NPs and interacting particles.

The influence of core/shell nanostructures on photovoltaic processes has been extensively studied in Ref. [6]. It has been shown that the presence of such NPs enhances the efficiency of dye-sensitized solar cells (DSSC) by 20%. Spectral-luminescent measurements revealed that while the optical density of the dye remained nearly unchanged, the fluorescence intensity increased twofold upon the addition of Ag NPs. The enhancement in DSSC efficiency is attributed to the LSPR effect of Ag NPs, which modifies the absorption

properties of the dye molecules. $Au/SiO_2/TiO_2$ particles have been used to increase the light absorption coefficient in solar cells. It has been demonstrated that the dielectric shell stabilizes the metallic core and prevents charge carriers' recombination that results in generation of more photons and growth of overall device performance [7, 8].

Core/shell NPs were also widely applied in photocatalysis. The authors of Ref. [9] synthesized Au NPs of various sizes and integrated them into core/shell structures with TiO_2 or SiO_2 shells. During the degradation of salicylic acid under visible light irradiation, samples containing Au NPs exhibited significantly higher catalytic activity compared to neat TiO_2. Notably, the highest activity was observed for Au NPs with a diameter of 3 nm, while for core/shell structures with SiO_2 shells, the best photocatalytic performance was achieved with 17 nm Au particles. In the first case, effective charge separation and the sensitization effect due to LSPR played a dominant role in enhancement of catalytic activity. In the second case, the dielectric shell of SiO_2 hindered charge carrier separation and the injection of hot electrons, suggesting that the observed increase in catalytic activity was primarily due to the local enhancement of the electric field around the Au NPs.

Additionally, Pt/CeO_2 and Ni/TiO_2 NPs have demonstrated high activity and stability in methane reforming and CO_2 conversion processes. The plasmon effect in such systems minimizes catalyst deactivation at high temperatures, which is particularly crucial for industrial applications. Moreover, the adjustable shell structure enables selective reaction control, making these materials promising candidates for sustainable chemistry [10, 11]. The authors of [12] also investigated the effect of Au NPs' size on the photocatalytic degradation of Methylene blue dye. Detailed microstructural studies concluded that the enhancement of photodegradation is predominantly driven by electron transfer mechanisms and the interface structure. This suggests that the photocatalytic efficiency is primarily influenced by the quantity and transport of charge carriers at the semiconductor/metal interface. However, unresolved questions remain regarding to the plasmon effect on the charge transfer processes.

This study presents theoretical and experimental investigations of the optical properties of core/shell NPs and their effect on the photocatalytic properties of TiO_2/rGO nanocomposite. Structures consisting of Ag NPs as cores and TiO_2 or SiO_2 as shells were selected. It was assumed that changes of the material of shell from a semiconductor to a dielectric could reveal whether the hot electrons of Ag NPs contribute to the enhancement of photocatalytic activity in TiO_2/rGO nanocomposites.

2. Materials and methods

The synthesis of Ag/TiO_2 NPs was performed according to method described in Ref. [13]. All reagents were of analytical grade and purchased from Sigma Aldrich. Silver NPs were prepared as cores by dissolving of 0.5 g of polyvinylpyrrolidone in 25 mL of ethylene glycol with the addition of 0.1 mmol of silver nitrate. The Ag NPs were separated from the ethylene glycol by centrifugation and washed twice sequentially with acetone and ethanol. Subsequently, 1 mL of TIPT ($Ti(OCH(CH_3)_2)_4$) was added to the ethanol solution of Ag NPs. According to dynamic light scattering data (Nanosizer S90, Malvern), the average size of silver NPs was 24±4 nm, while the size of core/shell structures was 44±8 nm (Fig. 1).

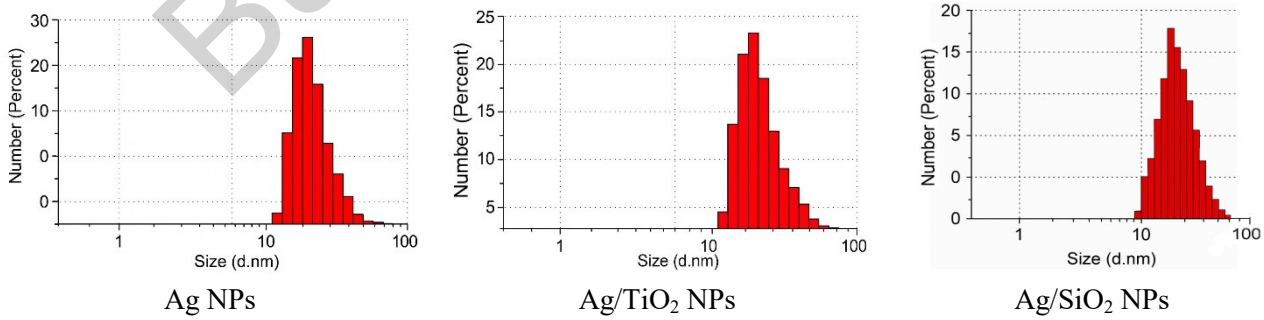

Fig.1. Size distribution of Ag NPs and core/shell NPs.

The synthesis of Ag/SiO_2 NPs followed to the procedure described in Ref. [14]. Tetraethyl orthosilicate (TEOS) was used as the SiO_2 precursor. The synthesized particles had cores with an average diameter of 24±4 nm, while the core/shell structures had an average diameter of 45±10 nm. The resulting solutions of core/shell NPs were incorporated into a TiO_2/rGO nanocomposite paste and mixed with a magnetic stirrer for

24 hours. The core/shell NPs concentration in the TiO_2/rGO nanocomposite was equal to 1 wt% according to the previous study [6]. For this concentration the greatest enhancement of photovoltaic parameters of the studied cells was recorded.

The TiO_2/rGO nanocomposite was synthesized via a hydrothermal method as described in Ref. [15, 16]. In particular, 40 mg of reduced graphene oxide (rGO) was sonicated in 160 mL of a water-ethanol mixture (1:3) for 1 hour. Subsequently, 400 mg of TiO_2 was added and the suspension was stirred for 2 hours. The light-gray suspension was autoclaved at 120°C for 24 hours, followed by cooling to room temperature. The TiO_2/rGO precipitate was centrifugated at 6000 rpm and washed with deionized water and ethanol. The obtained precipitate was dried at 60°C to produce a powder. To deposit TiO_2/rGO onto solid substrates, pastes were prepared from the resulting powder. For this, 300 mg of TiO_2/rGO powder was mixed with 2 mL of ethanol and mixed for 12 hours. The paste was spin-coated onto FTO substrates at 3000 rpm. The prepared TiO_2/rGO films, both with and without core/shell NPs, were annealed in an Ar atmosphere for 2 hours at 450°C.

The absorption spectra of the prepared samples were measured using a Cary-300 spectrophotometer (Agilent). The photocatalytic activity of the samples was evaluated by measuring the photoinduced current over 1 cm^2 of an illuminated area in a standard three-electrode cell with a potentiostat/galvanostat CS350 with an integrated EIS analyzer (CorrtestInstr.) according to the methodology described in [15]. Measurements were conducted in a 0.1 M NaOH electrolyte solution. A 300 W/cm^2 xenon lamp (Newport) was used as the light source. Impedance spectra were measured in steady-state mode. The amplitude of the applied signal was 15 mV and the frequency range was varied from 1 MHz to 100 mHz. To analyze the experimental curves and evaluate the electrotransport properties of the films, a simplified equivalent electrical circuit of the electrochemical cell was used (Fig. 2), which is a special case of the circuit from the Ref. [17].

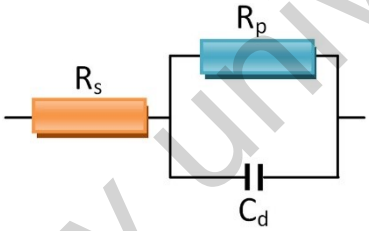

Fig. 2. Equivalent electrical circuit.

The optical properties of core/shell NPs were simulated using the finite-difference time-domain (FDTD) method, based on the Yee algorithm for solving Maxwell's equations. This algorithm involved discretizing of the computational domain into a rectangular grid, where electric fields were located along the grid boundaries, and magnetic fields were directed toward the cell centers.

The simulation domain was employed with Cartesian coordinate system with perfectly matched layer (PML) boundary conditions. To ensure maximum accuracy, a grid with an index of 8 and a step size of 0.5 nm was used. Grid refinement was achieved using the conformal0 method. Simulation parameters were set to 1000 femtoseconds and 300 K. Spherical Ag NPs with SiO_2 and TiO_2 shells were placed within the simulation domain. The radius of the Ag core was 13 nm, and the shell thickness was 5 nm. Material data for silver were sourced from [18], for SiO_2 from [13], and for TiO_2 from [19] and the open database refractiveindex.info. A total-field scattered-field (TF-SF) source was used as the radiation source. For NPs in a homogeneous medium, the incident radiation from the source represented a p-polarized plane wave propagating along the z-axis, with a wavelength range of 300–800 nm was used.

3. Results and discussion

The synthesized Ag/TiO_2 nanoparticles exhibited a spherical shape, as it was confirmed by SEM image (Mira 3LMU, Tescan). The absorption spectra of Ag and Ag/TiO_2 NPs revealed that before the shell synthesis, the absorption band of Ag NPs had a maximum at approximately 405 nm (Fig. 3). After coating with the TiO_2 shell, a bathochromic shift in the spectrum was observed. Additionally, from the short-wavelength region of the spectrum exhibits an absorption corresponding to the TiO_2, with the absorption edge located around ~380 nm. Similar data were obtained for Ag/SiO_2 NPs. The calculated optical properties and electric field intensity distributions around the studied NPs (Fig. 4) showed that the maximum of

calculated absorption band of Ag NPs exhibits at 380 nm. As experiments have shown, coating of the metal NPs with a shell caused a bathochromic shift in the absorption spectra. For Ag/SiO_2 NPs, the absorption maximum appeared at 390 nm, while for Ag/TiO_2, it shifted to 410 nm. The calculated absorption band positions correlated well with experimental data.

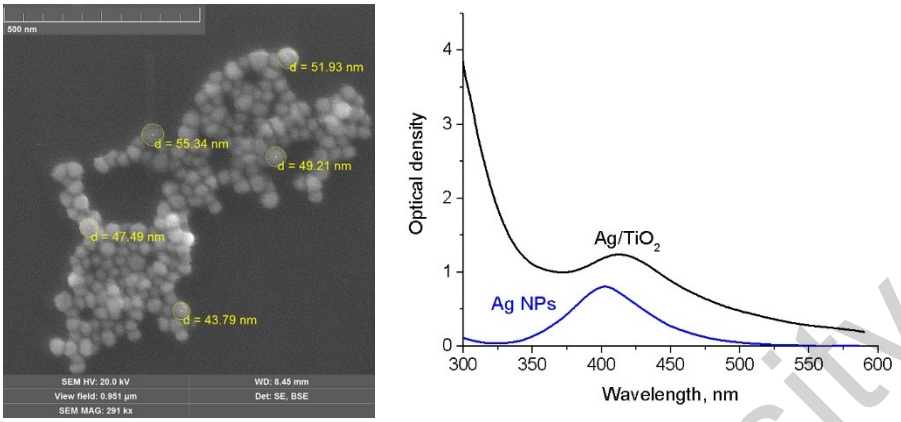

Fig. 3. SEM images of Ag/TiO_2 NPs (a) and (b) the absorption spectra of Ag and Ag/TiO_2 NPs.

The bathochromic shift in the calculated absorption spectra of NPs with the shell, relative to their absorption spectra in ethanol, can be attributed to the dependence of absorption plasmon NPs on the properties of the surrounding environment. According to Mie theory [1] the polarizability (α) of the metallic NPs is defined by the Clausius-Mossotti relation [20]:

$$\alpha = 4\varepsilon_0 \pi R^3 \frac{\varepsilon - \varepsilon_m}{\varepsilon + 2\varepsilon_m} \quad (1)$$

where ε is the permittivity of vacuum, ε_m is the dielectric constant of surrounding medium, ε is the dielectric function of the metall NP and R is the radius of spherical NP.

The intensity of absorption of light by the NPs (δ_{abs}) is proportional to the imaginary part of the polarizability [1]:

$$\delta_{abs}(\omega) \sim \mathrm{Im}[\alpha(\omega)] \quad (2)$$

I.e., the absorption maximum of NPs corresponds to the frequency at which the imaginary part of polarizability is maximal. Hence, it is seen that the optical properties of plasmon NPs are determined by both the properties of the environment and its individual properties. The quantum efficiency, defined as the ratio of emitted photons to absorbed photons, was also calculated (Fig. 4b).

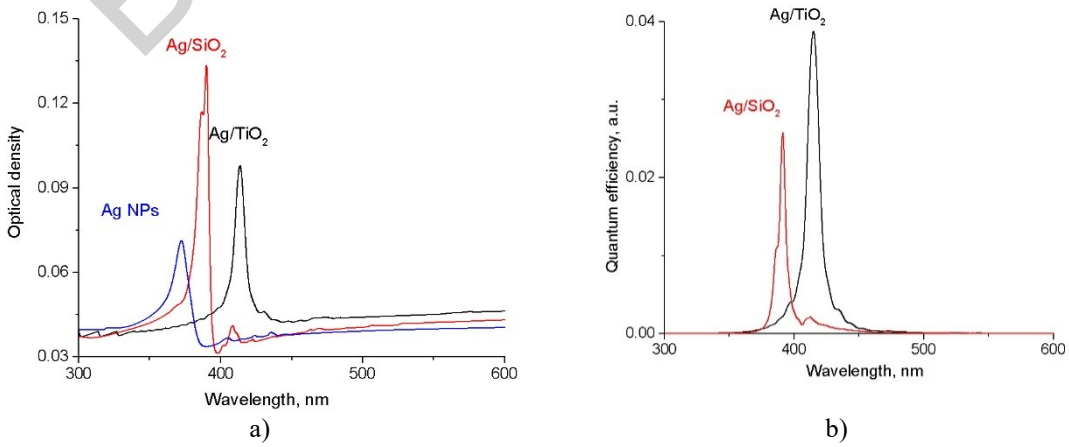

Fig. 4. Calculated absorption (a) and quantum efficiency (b) spectra of Ag and core/shell NPs.

The results showed that the quantum efficiency of Ag/TiO_2 NPs was approximately on 50% higher than that of Ag/SiO_2 NPs. This difference may be attributed to the fact that a greater number of free electrons are transferred from Ag NP to the semiconductor environment upon light irradiation compared to the SiO_2 layer. This hypothesis is supported by the 2D electric field intensity distribution patterns (Fig. 5).

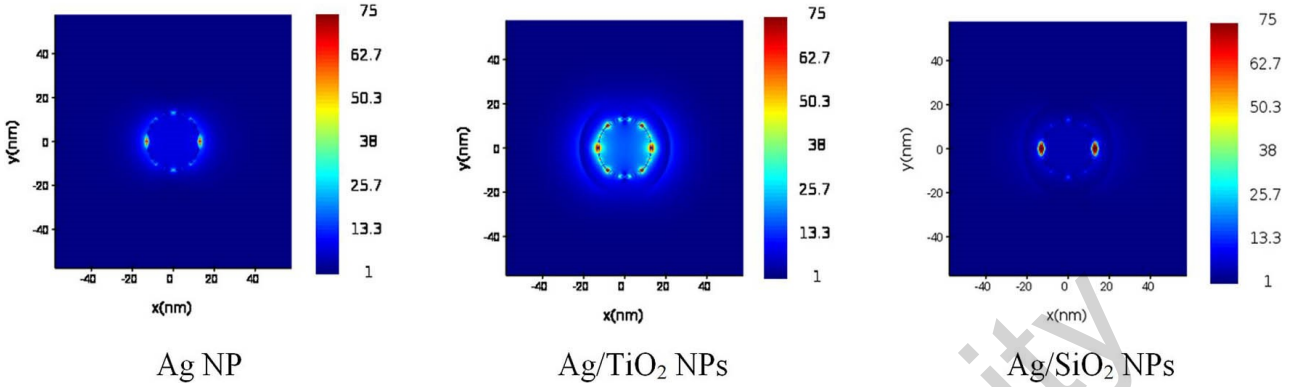

Fig. 5. 2D electric field intensity (in V/m) distributions around Ag and core/shell NPs.

The data revealed that the maximum electric field intensity is radially concentrated, predominantly near the surface of NPs along the OX direction. The magnitude of the field strength around the NP is varied from 1 to 75 V/m. For Ag/TiO_2 NPs, the electric field was more pronounced and uniformly distributed across the entire plasmon surface of NPs, unlike of Ag/SiO_2 NP.

Photocurrent measurements of the TiO_2/rGO nanocomposite with plasmon NPs confirmed the observed differences in optical properties and electric field distributions. The photocurrent density (Fig. 6) increased upon the addition of core/shell NPs to the TiO_2/rGO nanocomposite. For the pure TiO_2/rGO film, the current density was I=0.17 mA/cm^2, while it increased to I=0.45 mA/cm^2 for samples with Ag/TiO_2 NPs. In the case of Ag/SiO_2 NPs, the maximum photocurrent enhancement (1.7 times) was lower than that for Ag/TiO_2 (2.7 times). The photocurrent profile can be explained as follows: upon light irradiation, rapid photoinduced separation of electron-hole pairs occurs, resulting in a spike in the photocurrent curve. This is clearly visible for samples with core/shell NPs. This spike then diminishes as charge carriers migrate to the film surface. The subsequent decrease in photocurrent indicates that charge carriers recombination occurs within the film. The constant photocurrent level is achieved when the rates of charge carrier generation and recombination are balanced. During subsequent irradiation cycles the photocurrent increases with time and reaches saturation in the TiO_2/rGO samples. This shape of the curve could be resulted by the slow charge transport as well as the presence of traps in the TiO_2 and rGO, which leads to the gradual accumulation of charge carriers until the dynamic equilibrium was established [16]. The previously described behavior of the photocurrent curve was observed for nanocomposite samples with core/shell NPs. This may be due to the plasmon effect of silver NPs, which contributes to a more efficient separation of charge carriers and the enhanced local electromagnetic field and generation of hot electrons [15]. In all cases, a long-term relaxation of the amplitude of photocurrent pulses is observed, which indicates the presence of slow processes of accumulation of residual charges in the TiO_2/rGO structure between illumination cycles.

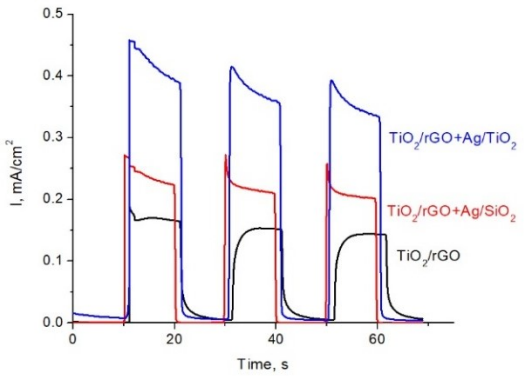

Fig. 6. Photocurrent profiles of the TiO_2/rGO nanocomposite with core/shell NPs.

The observed changes in the photocurrent value may be associated with an improvement in their charge-transport properties, data on which were obtained using impedance spectroscopy (Table 1). The electrophysical parameters were assessed using the methodology of Refs. [15,21], where τ_{eff} is the effective lifetime of an electron in a nanocomposite material; R_s characterizes the equivalent resistance of the film from the entire volume of the nanocomposite and the intercontact resistance between the layers. R_p corresponds to the resistance of charge carrier transfer at the interface between the layer under study and the electrode.

Table 1. Electrophysical parameters of TiO_2/rGO nanocomposite with Ag/TiO_2 and Ag/SiO_2 NPs

Sample	R_s, Ohm	R_p, Ohm	τ_{eff}, s
TiO_2	37.20	969.22	0.0078
TiO_2+ Ag/TiO_2	17.81	118.65	0.0051
TiO_2+ Ag/SiO_2	20.28	131.71	0.0033

The data indicate that nearly all parameters related to the resistance of nanocomposite films decrease in the presence of core/shell NPs. A significant reduction in recombination resistance (R_p) is observed for f Ag/TiO_2 NPs. Moreover, the shortest effective electron transit time was recorded. These results indicate that the addition of core/shell NPs effectively reduces the electron lifetime in the semiconductor, which enhances charge generation and separation, prevents recombination, and facilitates rapid electron migration and extraction from the semiconductor surface, enabling them to participate in photocatalytic reactions.

4. Conclusion

The results of this study demonstrate that the presence of Ag/TiO_2 and Ag/SiO_2 core/shell NPs enhances the photocatalytic activity of the TiO_2/rGO nanocomposite by 2.7 and 1.7 times, respectively. These changes can be attributed to improved charge transport properties in TiO_2/rGO and the potential injection of hot electrons from the metal NPs into the semiconductor. This process is notably hindered when a dielectric SiO_2 shell surrounds the Ag NPs.

The results of the studies show that the presence of Ag/TiO_2 and Ag/SiO_2 NPs enhances the photocatalytic activity of TiO_2/rGO nanocomposite by 2.7 and 1.7 times, respectively. The introduction of metal NPs into the composite increases the generation of charge carriers and promotes its separation, preventing their recombination, allowing them to participate in photochemical reactions. The possibility of injection of hot electrons from plasmon NPs as well as resonant energy transfer or charge tunneling from plasmon NPs also have to be taken into account. However, the latter processes are unlikely or significantly limited in this system. A more detailed study of the mechanism of the plasmon influence of metal NPs will be carried out by us in further studies.

The calculated with the FDTD method absorption spectra and electric field intensities revealed that the maximum absorption band of Ag NPs exhibits at 380 nm. Coating of the metal NPs with a shell induced a bathochromic shift in the absorption spectra, with the maximum absorption band at ~390 nm for Ag/SiO_2 and at 410 nm for Ag/TiO_2. These calculated results correlated well with experimental data. The maximum electric field intensity around plasmon NPs is radially concentrated, predominantly near the surface. For Ag/TiO_2, the electric field was more pronounced and distributed across the entire surface of the NPs. The quantum efficiency, defined as the ratio of emitted photons to absorbed photons, was approximately 50% higher for Ag/TiO_2 than for Ag/SiO_2 NPs. The findings of this study can be used to materials with enhanced photocatalytic and optoelectronic properties for applications in photoelectrochemical cells, hydrogen generation, organic compound photodegradation, and related areas.

Conflict of interest statement
The authors declare that they have no conflict of interest in relation to this research, whether financial, personal, authorship or otherwise, that could affect the research and its results presented in this paper.
CRediT author statement
Sharapov I.: software, calculations, writing – original draft; **Omarova G**.: visualization, validation; **Sadykova A**.: investigation, formal analysis; **Seliverstova E**.: conceptualization, methodology, resources, writing – review and editing. The final manuscript was read and approved by all authors

Funding

This work was supported by the Science Committee of the Ministry of Science and Higher Education of the Republic of Kazakhstan [Grant No. AP19680241].

References

1 Mayer K.M., Hafner J.H. (2011) Localized surface plasmon resonance sensors. *Chemical Reviews*, *111*, 3828–3857. https://doi.org/10.1021/cr100313v

2 Lin K.-T., Lin H., Jia B. (2020) Plasmonic nanostructures in photodetection, energy conversion and beyond. *Nanophotonics*, *9*(10), 3135–3163. https://doi.org/10.1515/nanoph-2020-0104

3 Barbillon G. (2019). Plasmonics and its applications. *Materials*, *12*(9), 1502. https://doi.org/10.3390/ma12091502

4 Ai B., Fan Z., Wong Z.J. (2022). Plasmonic–perovskite solar cells, light emitters, and sensors. *Microsystems Nanoengineering*, *8*, 5. https://doi.org/10.1038/s41378-021-00334-2

5 Kasani S., Curtin K., Wu N. (2019). A review of 2D and 3D plasmonic nanostructure array patterns: Fabrication, light management and sensing applications. *Nanophotonics*, *8*(12), 2065–2089. https://doi.org/10.1515/nanoph-2019-0158

6 Ibrayev N., Seliverstova E., Omarova G. (2020) The influence of plasmons of Ag nanoparticles on photovoltaics of functionalized polymethine dye. *Materials Today: Proceedings*, *25*, 39–43. https://doi.org/10.1016/j.matpr.2019.11.01

7 Chiozzia V., Rossi F. (2020) Inorganic–organic core/shell nanoparticles: Progress and applications. *Nanoscale Advances*, 2, 5090-5105. https://doi.org/10.1039/D0NA00411A

8 Rusdan N.A., Timmiati Sh.N., Yaakob Z., Lim K.L., Khaidar D. (2022) Recent application of core-shell nanostructured catalysts for CO_2 thermocatalytic conversion processes. *Nanomaterials*, 12(21), 3877. https://doi.org/10.3390/nano12213877

9 Turakova M., Salmi T., Eränen K., Warnå J., Murzin D.Y., Kralik M. (2015) Liquid phase hydrogenation of nitrobenzene. *Applied Catalysis A: General*. 499, 66-76. https://doi.org/10.1016/j.apcata.2015.04.002

10 Gawande M. B., Goswami A., Asefa T., Guo H., Biradar A.V., Peng D.-L., Zboril R., Varma R.S. (2015) Core–shell nanoparticles: Synthesis and applications in catalysis and electrocatalysis. *Chemical Society Reviews,* 44, 7540-7590. https://doi.org/10.1039/C5CS00343A

11 Das S., Pérez-Ramírez J., Gong J., Dewangan N., Hidajat K., Gates B.C., Kawi S. (2020) Core–shell structured catalysts for thermocatalytic, photocatalytic, and electrocatalytic conversion of CO2. *Chemical Society Reviews,* 49, 2937-3004. https://doi.org/10.1039/C9CS00713J

12 Lin L., Zhong Q., Zheng Y., Cheng Y., Qi R., Huang R. (2021) Size effect of Au nanoparticles in Au-TiO_2-x photocatalyst. *Chemical Physics Letters*, *770*, 138457. https://doi.org/10.1016/j.cplett.2021.138457

13 Afanasyev D.A., Ibrayev N.K., Serikov T.M., Zeinidenov A.K. (2016) Effect of the titanium dioxide shell on the plasmon properties of silver nanoparticles. *Journal of Physical Chemistry A*, *90*(4), 833–837. https://doi.org/10.1134/S0036024416040026

14 Alikhaidarova E., Afanasyev D., Ibrayev N., Nuraje N. (2022) Plasmonic enhanced polymer solar cell with inclusion of $AgSiO_2$ core-shell nanostructures. *Polymer Advanced Technologies*, *33*(3), 1000–1008. https://doi.org/10.1002/pat.5574

15 Seliverstova E., Serikov T., Nuraje N., Ibrayev N., Sadykova A., Amze M. (2024) Plasmonic effect of metal nanoparticles on the photocatalytic properties of TiO_2/rGO composite. *Nanotechnology*, *35*, 325401. https://doi.org/10.1088/1361-6528/ad3e02

16 Zhumabekov A., Seliverstova E., Ibrayev N. (2019). Investigation of photocatalytic activity of TiO2-GO nanocomposite. *Eurasian Physical Technical Journal*, 16(1(31)), 42–46. https://doi.org/10.31489/2019No1/42-46

17 Zhang B., Wang D., Hou Y., Yang S., Yang X. H., Zhong J. H., Liu J., Wang H. F., Hu P., Zhao H. J., Yang H. G. (2013). Facet-dependent catalytic activity of platinum nanocrystals for triiodide reduction in dye-sensitized solar cells. *Scientific Reports, 3,* 1836, https://doi.org/10.1038/srep01836

18 Johnson P.B., Christy R.W. (1972). Optical constants of noble metals. *Physical Review B*, *6*, 4370. https://doi.org/10.1103/PhysRevB.6.4370

19 Polyanskiy M.N. (2024). Refractive index.info database of optical constants. *Scientific Data*, *94*, 19. https://doi.org/10.1038/s41597-024-01102-5

20 Ibrayev N.Kh., Seliverstova E.V., Kanapina A.E. (2022) Transient absorption of gold nanoparticles of various diameters. *European Physical Technical Journal*, *19*(4), 73–77. https://doi.org/10.31489/2022No4/73-77

21 Adachi M., Sakamoto M., Jiu J., Ogata Y., Isoda S. (2006) Determination of parameters of electron transport in dye-sensitized solar cells using electrochemical impedance spectroscopy. *Journal of Physical Chemistry B*, *110*, 13872–13880. https://doi.org/10.1021/jp060976l

AUTHORS' INFORMATION

Sharapov, Ivan – Master's student, Buketov Karaganda University, Karaganda, Kazakhstan; https://orcid.org/0009-0000-6614-0338, ivan.sharapov.2001@mail.ru

Omarova, Gulden – PhD, Associate Professor, Head of the Department of Physics and Nanotechnology, Buketov Karaganda University, Karaganda, Kazakhstan; SCOPUS Author ID:56669661100, https://orcid.org/0000-0003-2900-2168; guldenserikovna@mail.ru

Sadykova, Aigul – Master (Sci.), Department of Physics and Nanotechnology, Buketov Karaganda University, Karaganda, Kazakhstan; SCOPUS Author ID: 57200382854; https://orcid.org/0000-0003-0148-3078; sadikova-aigul@mail.ru

Seliverstova, Evgeniya – PhD (Phys.), Associate Professor, Senior Research Fellow, Institute of Molecular Nanophotonics, Buketov Karaganda University, Karaganda, Kazakhstan; SCOPUS Author ID: 35323255400, https://orcid.org/0000-0002-9507-8825; genia_sv@mail.ru